ACS OMEGA

Open Access

http://pubs.acs.org/journal/acsodf

Review

Self-inducing Reactors for Bioengineering

Jian Gan, Huazong Liu, Jiajun Chen, Xingyan Li, Ganlu Li, Hui Li,* and Kequan Chen

Cite This: *ACS Omega* 2023, 8, 48613−48624

Read Online

ACCESS | Metrics & More | Article Recommendations

ABSTRACT: Packed tower reactors, mechanically stirred reactors, airlift reactors, and gas-self-inducing reactors are frequently utilized among the various types of reactors. Self-inducing reactors exhibit notable advantages owing to their simple structure, effective gas−liquid intermixing, and low energy requirements, rendering them highly suitable for bioengineering endeavors. The purpose of this analysis is to shed light on the use of self-inducing reactors in bioengineering by examining the following five parameters: critical speed, suction rate, volumetric mass transfer coefficient, power characteristics, and gas hold-up. Through a comprehensive analysis of the advancements achieved in these domains, it is possible to determine the challenges and opportunities that lie ahead in the realm of bioengineering.

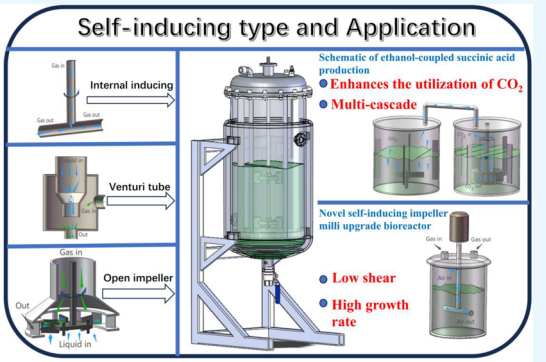

1. INTRODUCTION

Reactor systems are extensively utilized throughout diverse domains, including bioengineering, chemical engineering, sewage treatment, and metallurgy. There are several distinct types of reactors, including packed tower reactors, mechanically stirred reactors, airlift reactors, and gas-self-inducing reactors. In order to enhance the gas−liquid reaction process in packed tower reactors, mechanical stirring reactors, and airlift reactors, aeration devices such as gas distribution rings, pipelines, and porous plates are often integrated. Nevertheless, the incorporation of these components amplifies the total intricacy of the reactor installation, resulting in elevated energy consumption and an augmented likelihood of malfunction.[1] In contrast, self-inducing reactors have a simpler structure because the blades can simultaneously mix, agitate, and draw in the gas. This eliminates the need for an external gas supply apparatus and permits the recycling of unreacted gas multiple times within the reactor, thereby improving utilization efficiency.

Self-inducing reactors are therefore economically and practically feasible for industrial-scale reactions. These benefits have led to a growing interest in the self-inducing reactor for use in gas−liquid bioprocesses.[2] An extensive study has been carried out on self-inducing reactors, and Figure 1 provides a concise summary of the progression of their developmental stages, which range from single suction mode to multistructure suction mode. Moreover, computational fluid dynamics (CFD) has played a crucial role in furthering research on self-inducing reactors and expanding their applicability in a variety of fields.[3−5]

Research on reactor characteristics focuses predominantly on key parameters including critical speed,[6] suction rate,[7] power consumption,[8,9] gas hold-up, and volumetric mass transfer coefficient.[10,11] The investigation of these parameters is conducted by employing a combination of experimental methods, mathematical models, and numerical simulations. This comprehensive approach serves as the basis for the optimization of reactor design. The advent of CFD has made a noteworthy impact on the area, as it enables an extensive numerical model and analysis of the distribution of flow fields within the reactor. This is particularly beneficial in the context of gas−liquid two-phase flows, as it enhances the ability to see and analyze the distribution of gas and liquid phases. The use of this approach not only leads to a decrease in capital investment during the design phase but also improves the accuracy and reliability of the reactor.[12] As a result, CFD simulations enable more precise and efficient scale-up, which serves as the foundation for reactor design and optimization. The knowledge acquired from these investigations carries great importance in comprehending the structural configuration of self-inducing reactors and facilitating their industrial implementation.

2. SELF-INDUCING REACTORS

2.1. Types of Self-inducing Reactors. On the basis of the inspiratory principle, self-inducing reactors can be

Received: August 30, 2023
Revised: November 14, 2023
Accepted: November 17, 2023
Published: December 11, 2023

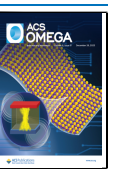

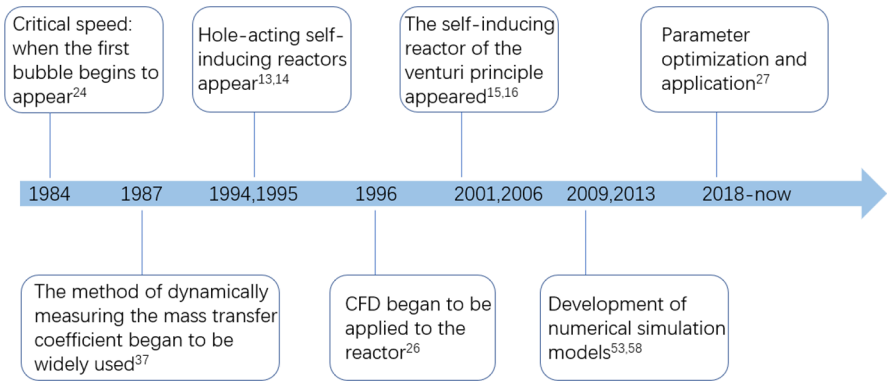

Figure 1. Timeline of self-inducing reactor development.

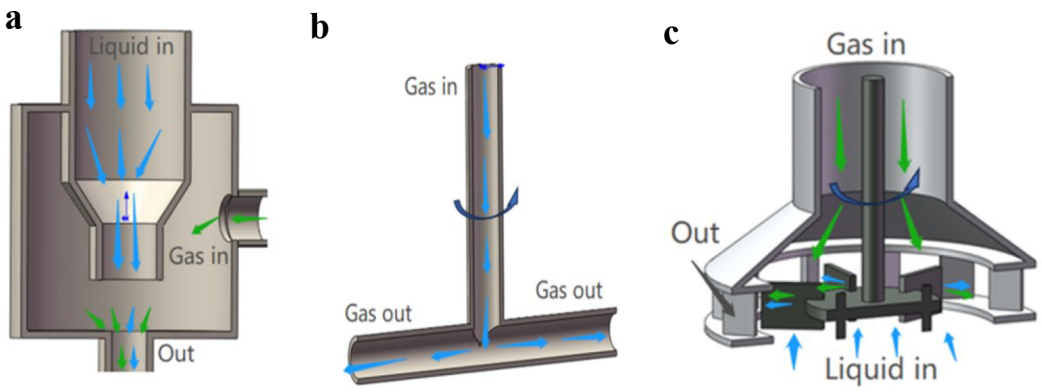

Figure 2. Some types of gas-inducing impellers. (a) The self-inducing impeller based on the Venturi tube principle comprises a contraction pipe and a gas−liquid mixing cavity. (b)The internal self-inducing impeller consists of a hollow shaft and self-inducing impeller. (c) The mechanically stirred self-inducing impeller with cavitation comprises a rotating impeller and a dispersing stator.

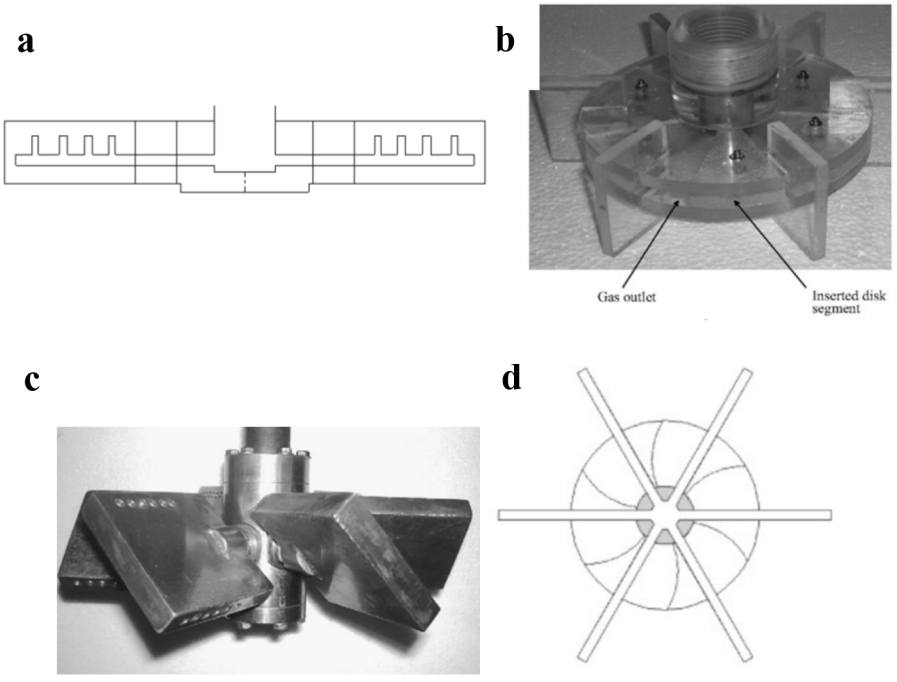

Figure 3. Improvement of self-inducing impeller design. (a) Six-blade concave self-inducing impeller. Reprinted with permission from ref 21. Copyright 1998 Elsevier B.V. License Number 5644001141792. (b) The self-inducing double disc impeller. Reprinted with permission from ref 22. Copyright 2008 Elsevier B.V. License Number 5643991096684. (c) Self-inducing inclined impeller. Reprinted with permission from ref 22. Copyright 2008 Elsevier B.V. License Number 5643991096684. (d) The hollow tube self-inducing impeller incorporating six circular tubes. Reprinted with permission from ref 23. Copyright 2009 Elsevier B.V. License Number 5643601243866.

https://doi.org/10.1021/acsomega.3c06484
ACS Omega 2023, 8, 48613−48624

categorized into three types: mechanically agitated self-inducing reactors with cavitation,[13,14] Venturi tube principle reactors, and hollow tube self-inducing reactors.[15−17] Figure 2 illustrates the schematic layout of reactors, displaying their structural layout.

The Venturi tube operates by utilizing a hydraulic pump to generate a high-speed liquid flow, which in turn draws gas into the reactor. The open blade impeller is commonly utilized for surface suction due to its uncomplicated structure and excellent suction efficiency. The suction mechanism utilized by the internal self-inducing impeller is comparable to cavity suction, primarily employed for internally suctioning reactors. Therefore, extensive research has been conducted on the open blade impeller and the internal self-inducing impeller, taking into account various working conditions.[18−20]

The self-inducing reactor, which is based on the Venturi tube principle, consists of a contraction pipe and a gas−liquid mixing cavity. The liquid phase flows through the pipeline at a certain velocity by utilizing an external hydraulic pump. As the liquid reaches the contraction pipeline, its speed increases, resulting in ejection from the pipeline mouth (see Figure 2a). The high-speed flowing liquid phase simultaneously drives the gas phase, resulting in the formation of a gas−liquid mixed phase that enters the reactor.[15] However, high shear stress poses a significant challenge in bioengineering applications.

The hollow impeller consists of a hollow shaft and an impeller, while the open impeller is composed of an impeller and a stator (see Figure 2b and 2c). According to eq 1, the fluid in motion is subjected to three types of energy: kinetic energy, gravitational potential energy, and pressure potential energy. The gas will be inhaled once the pressure difference generated during inhalation is overcome. As the impeller rotates, the fluid elements surrounding it acquire kinetic energy and generate negative pressure. Consequently, the gas is drawn into the reactor due to the pressure difference.

$$\frac{1}{2}\rho v^2 + \rho g h + P = c \tag{1}$$

ρ: Fluid density in kg·m^{-3}; v: Fluid velocity in m·s^{-1}; g: Gravity acceleration in m·s^{-2}; h: Fluid unit position in m; P: Pressure at a certain point in a fluid in Pa; c: Dimensionless constant.

Researchers have made significant progress in the construction of self-inducing impellers, building upon the previously specified suction approach. In their study, Forrester et al.[21] investigated a self-inducing impeller with six concave blades. The blades were hollow and had apertures on their surface to facilitate coupling with the hollow shaft. The structural diagram is depicted in Figure 3a. Murthy et al.[22] enhanced the self-inducing double disc impeller (MDD) and conducted experiments with the self-inducing inclined impeller (PBTD). The enhanced MDD is comprised of upper and lower discs that are interconnected and fastened together by vertically dispersed impellers. The gas phase enters the center cavity of the disc by way of a hollow shaft, and then it is spread throughout the reactor vessel by means of dispersed blades, as shown in Figure 3b. The PBTD blade exhibits internal hollowing, with suction being facilitated by lateral holes, as seen in Figure 3c. Ju et al.[23] presented a unique design methodology for self-inducing impellers in order to mitigate the reduction in speed. This strategy involves the integration of six circular tubes that extend radially from the axis of the impeller. The circular tubes are interconnected with the hollow shaft through connectors, and there are apertures located on the surface of the circular tubes. Various impeller blades are integrated beneath the circular tube in order to attain an optimal self-inducing impeller design. The structural schematic diagram is depicted in Figure 3d.

2.2. Self-inducing Reactor Parameter Characteristics.

The field of self-inducing reactors includes the examination of several significant attributes, such as critical speed, suction rate, volumetric mass transfer coefficient, power characteristics, and gas hold-up. The reaction process and the state within the reactor are directly influenced by these characteristics, which exhibit a strong correlation with the reactor's structure and the structural parameters of the self-inducing impeller. The gas-inducing reactors possess two distinct variables, namely the critical speed and suction rate. Tanaka et al.[24] defined the critical speed, which refers to the speed at which the initial bubble becomes perceptible.

Presently, the majority of reactor investigations use a combination of theoretical analysis and experimental validation. However, due to notable progress in the fields of fluid mechanics and computer technology, computational fluid dynamics (CFD) has emerged as a promising approach. CFD is a research approach that is partially theoretical in nature and is commonly employed in the study of reactors. It is often used in conjunction with experimental research to provide useful insights into the modeling and optimization of reactors. Numerous theories and research methods have been developed by scholars in the field of self-inducing reactors, which have significantly aided in the resolution of flow field and mass transfer issues within the reactor. This combination of semi-theory and experiment has considerably decreased testing time while improving accuracy and efficiency in following reactor improvement designs.[25] The study conducted by Harvey et al.[26] utilized CFD technology to analyze and forecast the two-dimensional flow patterns occurring within stirred reactors. This enabled the researchers to effectively visualize the interior flow fields of these reactors. This work presents a comprehensive review of the theoretical advancements made in the study of these parameters as well as the application of CFD.

2.2.1. Critical Speed. The critical speed of self-inducing reactors with gas-phase multiphase flow is of the utmost significance since it directly influences the effectiveness of the self-inducing impeller. The power consumption of the reactor is directly affected by the rotating speed, and throughout the scale-up design process, higher speeds lead to higher costs. Furthermore, increased rotational speeds result in significant shear stresses, which have the potential to induce mortality in microorganisms present within the culture, thereby impacting the overall quality of the product. Hence, the identification of strategies to reduce the critical speed has considerable significance in the context of bioengineering applications pertaining to self-inducing reactors.

The critical speed of a system is influenced by several elements, such as the structural characteristics of the impeller, the properties of the fluid in the liquid phase, and the specific configuration of the impeller type. These factors have a direct or indirect influence on the critical speed. The study conducted by Zhang et al.[27] revealed that the critical speed is indirectly influenced by the presence and density of solid particles, whereas bigger solid particles lead to a decrease in the critical speed. Research was undertaken by Murthy et al.[22] to investigate the impact of various impeller designs and the

https://doi.org/10.1021/acsomega.3c06484
ACS Omega 2023, 8, 48613−48624

Table 1. Critical Speed and Suction Rate

Ref	Critical speed	Suction rate
Heim et al.[20]	$Fr^* = Fr\frac{d}{h_0}\ \frac{N^2d^2}{g(h-y)}$	---
Evans et al.[28]	$N_c = \sqrt{\frac{gh_0}{2[\pi R(1-K_0)]^2(C_p-1)}}$	---
Martin et al.[29]	---	$Q = C_oSK_1[2g(-h_0)(\rho_q/\rho_p)]^{1/2} - 0.00085K_1$
Forrester et al.[21]	---	$Q = \frac{4\pi(r_d^3-S^3)}{3}\frac{1}{t_d} = \frac{4\pi(r_d^3-S^3)}{3}\frac{uC_P^{1/2}}{(r_d+s)}$
Sawant et al.[30]	$\frac{N_c^2d^2}{gh_0}(\mu/\mu_w)^{-0.11} = 0.21$	---
Ju et al.[23]	$N_c = \frac{\sqrt{2gh_0}}{\pi dK}$	$Q = S\left(\left[\frac{\rho_q(1-\alpha_p)}{\rho_p} + \alpha_p\right][(\pi dNK)^2 + 2h_{f1} - 2gh_0] - 2h_{f2}\right)^{\frac{1}{2}}$

presence of solid particles on the critical speed. The critical speed values were acquired by CFD simulations and then compared to the critical speeds determined through the utilization of a magnetic sensor. The findings exhibited a high level of concordance between the two. Previous studies have examined the relationship between critical speed, suction rate, operational circumstances, and structural characteristics of self-inducing reactors, as described in Table 1. Heim et al.[20] describes the beginning of self-inducing impeller suction through Fr^*, and defines the critical Fr^* of different impellers to describe the critical speed of self-inducing impeller, the higher Fr^*, the higher the critical speed of the impeller. Evans et al.[28] proposed a model for blade slip coefficient and pressure coefficient that predicts critical speed with precision. In their research, Martin et al.[29] proposed the use of a dimensionless experimental constant, denoted as K_1, in order to address the discrepancy seen between suction rate measurements and theoretical predictions. In their study, Forrester et al.[21] made improvements to the model used for the porous outlet impeller. These enhancements focused on addressing the beginning circumstances and the dynamic pressure loss coefficient. As a consequence of these modifications, the researchers were able to achieve reductions in both theoretical and experimental errors. Sawant et al.[30] took into account viscosity as a factor alongside structural characteristics while investigating critical speed, ensuring an error margin of less than 10%. The model proposed by Ju et al.[23] incorporates the principles of energy conservation to determine the critical speed and suction rate in gas suction pipe research. This model disregards any losses in turbulent kinetic energy, hence expanding its potential applications in this field.

In addition to analyzing the effects of self-induced structure and impeller combinations on critical speed, a considerable number of academics have also conducted research on the mathematical model pertaining to critical speed. In the field of single-phase fluid mechanics, it is commonly accepted that, in the absence of frictional losses, the initiation of gas intake occurs when the pressure difference ΔP resulting from impeller spinning surpasses the pressure drop.[31] The aforementioned relationship may be mathematically represented by the subsequent equation:

$$\Delta P = \rho_q g h_0 \tag{2}$$

ΔP: Pressure drop in Pa; ρ_q: Liquid density in kg·m^{-3}; h_0: Liquid depth in m.

The pressure coefficient C_P is a significant metric in the gas self-inducing system since it denotes the ratio between the dynamic head and the static head.[32] The equation for determining this coefficient is as follows:

$$C_p = \frac{\Delta P}{\frac{1}{2}\rho_q V_{tip}^2} = \frac{\Delta P}{\frac{1}{2}\rho_q(\pi N d)^2} \tag{3}$$

C_P: Pressure coefficient, dimensionless; V_{tip}: Speed of impeller tip in m·s^{-1}; d: Impeller diameter in m; N: Impeller speed in r·min^{-1}.

Combining eqs 2 and 3 yields the following relationship between the critical speed, N_C, and the pressure coefficient, C_P:

$$N_c = \frac{1}{\pi d}\sqrt{\frac{2gh_0}{C_p}} \tag{4}$$

N_C: Critical speed in r·min^{-1}.

In order to create a mathematical model, Ju et al.[23] explored the theory of energy conversion between gas intake and gas evacuation. The pressure differential between the pressure P_a at the gas suction hole and the pressure P_1 at the gas outlet hole is used to compute the motive force of gas suction. An energy study reveals:

$$gh_0 + \frac{P_a}{\rho_q} = \frac{P_1}{\rho_q} + \frac{1}{2}u^2 + h_{f1} \tag{5}$$

h_{f1}: Energy loss in turbulent liquid; P_a: Gas suction inlet pressure in Pa; P_1: Pressure at the gas outlet in Pa; u: Gas–liquid relative velocity at the air outlet $u = \pi dNK\ (0 < K < 1)$ in m·s^{-1}; K: Velocity loss coefficient.

When $P_a = P_1$, the first bubble is observed.

When inducing air, $P_a > P_1$

$$P_a - P_1 = \frac{1}{2}\rho_q u^2 + \rho_q h_{f1} - \rho_q g h_0 \tag{6}$$

Finishing is available:

$$N_c = \frac{\sqrt{(2gh_0 - h_{f1})}}{\pi dK} \tag{7}$$

As the energy loss in a turbulent liquid is negligible and can be ignored, so:

$$N_c = \frac{\sqrt{2gh_0}}{\pi dK} \tag{8}$$

https://doi.org/10.1021/acsomega.3c06484
ACS Omega 2023, 8, 48613−48624

The mathematical model determines that the diameter and immersion depth of the impeller directly impact the critical speed of a self-inducing impeller. The relationship between the critical speed and impeller diameter is inverse, indicating that an increase in impeller diameter leads to a decrease in critical speed. Moreover, it can be observed that the critical speed exhibits a direct relationship with the immersion depth, implying that an increase in immersion depth results in a corresponding increase in critical speeds. When the diameter of the self-inducing impeller is increased, the distance between the air exit and the rotating center is correspondingly greater. As a result, the linear tip speed at the air exit is greater compared to the same speed achieved with a smaller impeller diameter. Conversely, augmenting the immersion depth of the self-inducing impeller leads to an elevated pressure differential that must be overcome during gas intake. The impeller's liquid microelements necessitate a greater amount of kinetic energy in order to surpass the pressure at the gas exit. Consequently, it is necessary to augment the rotational speed of the impeller in order to guarantee that the liquid phase contained within the impeller obtains sufficient kinetic energy.

2.2.2. Suction Rate. The analysis of the suction rate is of utmost importance in the study of self-inducing reactors, as it serves as a direct indicator of the reactor's suction performance and its ability to disperse gas and liquid phases. The suction rate is predominantly affected by the pressure differential and the gas dispersion capability during the self-inducing impeller's rotation.[31]

Through analysis of the fundamental principles behind the suction performance of self-inducing reactors, it has been found that the suction process is propelled by a pressure disparity that arises from the rotational motion of the self-inducing impeller. The dimensions and configuration of the impeller blades are influential factors in the determination of both the pressure differential and the capacity for gas−liquid dispersion. The influence of impeller design, solid particle size, and solid particle density on the suction rate has been examined in previous research conducted by Murthy et al.[22] The results of their study demonstrated a clear correlation between the rate of suction and the size and density of particulate matter. The presence of larger and denser solid particles was shown to be positively correlated with greater critical speeds and enhanced suction rates. In a study conducted by Deshmukh et al.,[32] it was shown that the suction rate is positively correlated with the increase in both the opening area and the blade angle of the impeller design.

Ju et al.[23] did research in the field of optimization design for self-inducing impellers. They constructed a mathematical model with the aim of determining the suction rate.

The determination of the gas suction flow rate Q may be achieved by employing the Bernoulli equation, which establishes a relationship between the gas suction hole and the gas outlet hole.

$$\frac{P_1}{\rho_p} + \frac{1}{2}\left(\frac{Q}{S}\right)^2 + h_{f2} = \frac{P_a}{\rho_p} \tag{9}$$

Q: Gas suction rate in $m^3 \cdot h^{-1}$; S: Air outlet area in m^2; h_{f2}: Energy loss in the flow process.

Finishing is available:

$$Q^2 = 2S^2\left(\frac{P_a - P_1}{\rho_p} - h_{f2}\right) \tag{10}$$

Through combination of eqs 6, 9, and 10, a comprehensive equation can be obtained:

$$Q = S\left(\left[\frac{\rho_q(1-\alpha_p)}{\rho_p} + \alpha_p\right][(\pi dNK)^2 + 2h_{f1} - 2gh_0] - 2h_{f2}\right)^{1/2} \tag{11}$$

According to eq 11, it is advantageous to increase the stirring speed N or the impeller diameter d at the air outflow in order to increase the gas suction rate. In contrast to the mathematical model of critical speed, the model for suction rate incorporates numerous influencing factors, such as the interaction between the gas and liquid phases. As a consequence, the model's error is substantial, and it becomes more difficult to anticipate the critical speed.

With the development of CFD, the prediction of suction rate has become crucial to model development.[33] Murthy et al.[34] utilized an iterative method to calculate the gas suction rate, investigated the effect of impeller design and multiphase suction rate, and employed CFD simulations to predict the suction rate of self-inducing reactors. In addition, the combination of impellers has a significant impact on the suction rate. The axial flow of the blade beneath the self-inducing impeller is superior to the radial flow. Under the same rotational speed, the upward axial flow increases the suction rate of the impeller. During the rotation of the self-inducing impeller, the gas−liquid dispersion ability is limited, leading to the accumulation of gas within the liquid phase. These gas accumulations frequently cause cavitation in the low-pressure regions of the impeller, impeding the development of the extraction rate. The upward axial flow generated by the lower stirring paddle facilitates the discharge of bubbles accumulated in the low-pressure region of the self-inducing impeller through the air outflow. This indirectly improves the self-inducing impeller's gas−liquid dispersion capability and mitigates the cavitation phenomenon, thereby increasing the suction rate.

2.2.3. Volumetric Mass Transfer Coefficient. The volumetric mass transfer coefficient (k_La) holds significant importance in the analysis of reactors, as it serves as an indicator of mass transfer efficiency and exerts a direct impact on the reaction rate occurring within the reactor. The gas−liquid mass transfer process is that the gas molecules diffuse from the gas phase through the gas and liquid films to the bulk liquid. Conventional mechanically stirred reactors generally exhibit a relatively low gas−liquid mass transfer coefficient, which therefore leads to reduced reaction rates. Moreover, when the size of the reactors is increased, there is a drop in the total actual mass transfer coefficient. In order to improve the efficiency of mass transfer and stimulate higher response rates, it is often necessary to employ a supplementary aeration and gas−liquid dispersion apparatus.[35] Nevertheless, this methodology not only introduces intricacies to the apparatus but also amplifies the aggregate consumption of power. The reactor, which possesses a distinctive construction, effectively tackles these issues by simultaneously inducing gas into the reactor and facilitating stirring. The aforementioned design presents a novel approach that effectively enhances the volumetric mass transfer coefficient in the reactor, resulting in improved reaction rates.

https://doi.org/10.1021/acsomega.3c06484
ACS Omega 2023, 8, 48613−48624

Numerous scholars have undertaken comprehensive investigations into enhancing the mass transfer efficiency of self-inducing reactors. The impact of various gas−liquid phase types on mass transfer was investigated by Zieverink et al.[36] The researchers conducted tests to assess the mass transfer coefficient. The researchers also examined the impact of critical rotational speed, suction rate, rotational speed, gas−liquid turbulence intensity, and fluid characteristics (Reynolds number and Schmidt number) on the rate of gas−liquid mass transfer. Linek et al.[37] utilized a dissolved oxygen probe to quantify alterations in the concentration of dissolved oxygen in the liquid phase. This approach, which involves unsteady dynamic measurements, has been extensively exploited in the past for the purpose of determining k_La.

The volumetric mass transfer coefficient, k_La, for gas−liquid systems, as determined by the physical unsteady-state dynamic measurement approach outlined earlier, is based on the assumption of a flow state characterized by complete mixing. Nevertheless, the attainment of a completely homogeneous flow condition in real-world reactor applications poses significant difficulties, resulting in a certain level of imprecision in measurements. In addition to the physical unsteady-state approach, chemical steady-state methods are also employed. These include the sulfite oxidation method and the absorption of carbon dioxide by an aqueous solution of sodium hydroxide. The advantage of chemical methods is that they do not rely on the supposition of a completely mixed flow state and can neglect the impact of the gas phase flow in the liquid phase. However, chemical approaches are often more appropriate for systems that do not readily coalesce.[38] The investigation of the volumetric mass transfer coefficient encompasses the utilization of both physical and chemical methodologies, which are extensively applied.[21] Moreover, a significant body of research has been undertaken to investigate the many elements that impact the volumetric mass transfer coefficient. The k_La value is subject to the effect of two key factors: the liquid film mass transfer coefficient, k_L, and the specific surface area, a. Numerous studies have been undertaken by researchers in order to raise the particular surface area, denoted as "a". As an illustration, Sharma et al.[39] successfully produced nanobubbles by utilizing an ejector, resulting in a significant reduction in bubble diameter. Nanobubbles demonstrated a significant enhancement in the volumetric mass transfer coefficient, with values ranging from 2.2 to 3.8 min^{-1}, when compared to microbubbles. In their research, Lakhdissi et al.[40] included minute solid particles in the bubble column reactor with the aim of decreasing the gas−liquid interfacial area (a) and increasing the mass transfer coefficient (k_L). The enhancement of the volumetric mass transfer coefficient may be achieved by altering the reactor's construction, the adjustment of its operating conditions, and the modification of its internal components. Similar to the research on critical speed and suction rate, modifying the impeller type, impeller combination form, and geometric dimension also affects the volumetric mass transfer coefficient. In their study, Yu et al.[41] examined the relationship between impeller diameter, immersion depth, and mass transfer coefficient in a self-inducing reactor:

$$k_La = 1.212\left(\frac{P}{V_q}\right)^{0.0816} v^{0.692}\left(\frac{h_0}{d}\right)^{-0.390} \tag{12}$$

V_q: Liquid volume in m^3.

2.2.4. Power Characteristics. While ensuring optimal reactor performance, power consumption is a crucial parameter to consider, particularly for large-scale industrial apparatuses, where excessive power consumption can be expensive. Additionally, lower power consumption increases the reactor's efficiency and utilization.

The majority of the reactor's power consumption is attributable to the flow mixture within the reactor, which is influenced by a variety of factors, including the reactor's structure, impeller design, liquid properties, and blade configuration. In general, gas inhalation reduces energy consumption relative to non-gas inhalation. This is due to the fact that when gas is drawn into the impeller, the gas under impeller shear reduces the mixing density, resulting in a lower power consumption per unit volume and a lower overall power consumption.[42] Patil et al.[43] examine the design of a multiple-impeller self-inducing system and find that at the same gas hold-up, the power consumption is less when the bottom blade is 45°PBTU (pitched-blade upflow turbine). Some studies explored the impact of Reynolds number, fluid viscosity, and impeller stator on power consumption in both Newtonian and non-Newtonian fluids.[44] Power consumption was found to increase with viscosity. Baczkiewicz et al.[45] investigated the hollow tube impeller power consumption model. Their research improved our understanding of the dynamics of power consumption in the reactor system.

$$\frac{P_p}{V_q} = 0.62N^{3.44}\left(\frac{Q}{V_q}\right)^{-0.31}\left(\frac{d}{D}\right)^{4.48} n_1^{1.07} \tag{13}$$

P_p: Power consumption during suction in W; D: Reactor diameter in m; n_1: Number of blades.

In their work, Jafari et al.[46] investigated the correlation between the power number of a self-inducing impeller and the Reynolds number at various speeds. The power number has a negative correlation with the Reynolds number as it increases. The power number is mainly related to impeller diameter (d), rotating speed (N), viscosity (μ), and density (ρ) and increases with the increase of d, N, μ, and ρ.

$$N_P = \frac{P}{\rho N^3 d^5} \tag{14}$$

$$N_{\mathrm{Re}} = \frac{\rho N d^2}{\mu} \tag{15}$$

N_p: Power number, dimensionless; N_{Re}: Reynolds number, dimensionless; μ: Viscosity in $Pa{\cdot}s^{-1}$.

The aforementioned models can be classified as empirical formulas, and their practical utility is subject to certain constraints. Hence, it is necessary to make parameter adjustments for various types of self-inducing impellers.

2.2.5. Gas Hold-up. In conventional mechanically stirred reactors, the presence of aeration equipment is necessary to facilitate the introduction of gas, hence establishing a direct correlation between gas hold-up and gas flow. In the framework of self-inducing reactors, it is observed that when the rotating speed of the impeller surpasses the critical speed, there is an automatic inflow of gas into the reactor. The gas hold-up in self-inducing reactors is significantly impacted by the suction rate, resulting in self-inducing impellers with a higher gas hold-up demonstrating superior suction performance.[47] When bubbles enter the liquid phase, they are

https://doi.org/10.1021/acsomega.3c06484
ACS Omega 2023, 8, 48613−48624

dispersed in the reactor under the shear dispersion of the impeller. Reduced bubble sizes yield enhanced dispersion uniformity and heightened vulnerability to turbulence, thus resulting in prolonged residence durations within the reactor and increased gas hold-up. The primary objective of enhancing the gas hold-up in self-inducing reactors is to enhance their suction performance and gas−liquid dispersion capability. There are several techniques available for the measurement of gas hold-up, such as the volume expansion method, pressure difference method, and conductivity probe method.[48,49] The utilization of high-precision X-ray imaging studies enables the quantification of the gas hold-up distribution within self-inducing reactors, hence facilitating the examination of various hydrodynamic characteristics. The utilization of this measuring approach has the potential to validate the findings derived from CFD simulations pertaining to gas hold-up.[50]

The gas hold-up in self-inducing reactors is influenced by the suction rate of the self-inducing impeller. Indirectly, the suction rate is influenced by factors that also have an impact on the gas hold-up. Gas hold-up in a double-layer self-inducing stirred reactor is influenced by several factors, including fluid characteristics, gas−liquid flow rate, operating temperature, geometric structure of the stirring paddle, stirring speed, and bubble size.[51,52] In a typical scenario, the gas hold-up exhibits a decline as the immersion depth increases, with all other factors remaining constant. The generation of upward axial flow by the bottom blade results in an enhancement of the suction rate, leading to an improvement in the gas hold-up.

In conclusion, the critical speed of a system is primarily influenced by the diameter of the impeller and the depth of immersion. Specifically, the critical speed decreases as the impeller diameter grows, while it increases as the immersion depth increases. The mass transfer coefficient is influenced by both bubble diameter and liquid viscosity. Specifically, the coefficient rises as the bubble diameter decreases and drops as the viscosity of the liquid increases. The primary parameters that influence gas hold-up, suction rate, and power consumption are the diameter and speed of the impeller. The gas hold-up, suction rate, and power consumption exhibit a positive correlation with both impeller diameter and rotational speed.

2.3. CFD Application of Self-inducing Reactors. In the study of two-phase flow in reactors, the Eulerian−Eulerian and Eulerian−Lagrange approaches are two of the most common techniques. The primary distinction between these techniques is how they handle dispersed phases in two-phase flow. The dispersed phases are calculated using the same coordinate system as the continuous phase in the Eulerian−Eulerian method. The Eulerian−Lagrange method, on the other hand, requires solving equations for a large number of dispersed phases in a Lagrange coordinate system, which can be computationally intensive. When the reactor is a two-phase gas−liquid system, the Euler−Euler method is typically employed because it provides a suitable framework for capturing the behavior of the dispersed gas phase.[53] In the Eulerian−Eulerian approach:

The conservation of mass equation:

$$\frac{\partial}{\partial t}(\alpha_q\rho_q) + \nabla\cdot(\alpha_q\rho_q\vec{v}_q) = \sum_{p=1}^{n}(\dot{m}_{pq} - \dot{m}_{qp}) + S_1 \tag{16}$$

S_1: Quality source term in kg·(m^3·s)$^{-1}$; $\dot{m}_{pq}$ and $\dot{m}_{qp}$: Mass flow rate between two phases in kg·s^{-1}; t: Time in s; α: Phase hold-up in %; p and q: Subscripts p and q denote gas phase and liquid phase.

Momentum transfer equation:

$$\frac{\partial}{\partial t}(\alpha_q\rho_q\vec{v}_q) + \nabla\cdot(\alpha_q\rho_q\vec{v}_q) = -\alpha_q\nabla p + \nabla\cdot\overline{\tau}_q + \alpha_q\rho_q\vec{g} + \sum_{p=1}^{n}(\vec{R}_{pq} + \dot{m}_{pq}\vec{v}_{pq} - \dot{m}_{qp}\vec{v}_{qp}) + (\vec{F}_q + \vec{F}_{lift,q} + \vec{F}_{wl,q} + \vec{F}_{vm,q} + \vec{F}_{td,q}) \tag{17}$$

$\overline{\tau}_q$: Stress tensor of q phase, dimensionless.

$$\overline{\tau}_q = \alpha_q\mu_q(\nabla\vec{v}_q + \nabla\vec{v}_q^{\mathrm{T}}) + \alpha_q\left(\lambda_q - \frac{2}{3}\mu_q\right)\nabla\cdot\overline{v}_q\overline{I} \tag{18}$$

μ_q: Shear viscosity in Pa·s^{-1}; λ_q: Bulk viscosity in Pa·s^{-1}; $\vec{F}_q$: External forces in N; $\vec{F}_{lift,q}$: Lift force in N; $\vec{F}_{wl,q}$: Wall slip force in N; $\vec{F}_{td,q}$: Turbulent dispersion force in N; $\vec{R}_{pq}$: Interphase drag in N.

The stirring paddle induces unpredictably turbulent flow patterns within the flow field of the reactor, resulting in a highly complex flow environment. In processes involving significant turbulence, the intensive shear effects further influence the flow characteristics and mass transfer rates. Therefore, it is essential to choose an appropriate turbulence model when simulating and predicting the behavior of a reactor. Reynolds stress models and vortex viscosity models are the two categories of turbulence model research. The vortex viscosity models are frequently used and include the conventional k-ε model, the improved RNG k-ε model, and the realizable k-ε model. Standard k-ε models and RNG k-ε models are currently more prevalent. The standard k-ε model is founded on the assumption of completely developed turbulence and is frequently appropriate for simulating high Reynolds number reactors. The RNG k-ε model modifies the coefficients of the standard k-ε model through theoretical analysis, thereby enhancing its applicability in numerous situations.

The standard k-ε model includes a turbulence dissipation rate ε that represents the turbulent kinetic energy consumed per unit of time. This is its system of control equations:[54]

Equation of k:

$$\frac{\partial}{\partial t}(\rho\mathrm{k}) + \nabla\cdot\left(\rho\mathrm{uk} - \left(\mu_{eef} + \frac{\mu_t}{\sigma_k}\right)\nabla\mathrm{k}\right) = G_b + G_k - \rho\varepsilon - Y_m + S_k \tag{19}$$

Equation of ε:

$$\frac{\partial}{\partial t}(\rho\varepsilon) + \nabla\cdot\left(\rho\mathrm{u}\varepsilon - \left(\mu_{eef} + \frac{\mu_t}{\sigma_\varepsilon}\right)\nabla\varepsilon\right) = \frac{\varepsilon}{\mathrm{k}}(C_{\varepsilon 1}(G_k + G_b) - C_{\varepsilon 2}\rho\varepsilon) + S_\varepsilon \tag{20}$$

$$\mu_t = \rho C_\mu\left(\frac{k^2}{\varepsilon}\right) \tag{21}$$

k: Turbulence kinetic energy in J·kg^{-1}; ε: Turbulence dissipation rate in m^2·s^{-3}; σ: Turbulent Prandtl number; G_K: Turbulence kinetic energy produced by average velocity gradient in J·kg^{-1}; G_b: Turbulence kinetic energy produced by buoyancy in J·kg^{-1}; Y_m: Influence of wave expansion on

https://doi.org/10.1021/acsomega.3c06484
ACS Omega 2023, 8, 48613−48624

turbulent dissipation rate; S_k: Source term of k equation; S_ε: Source term of ε equation; C_ε: Additional generating term of equation; μ_{eef}: Effective viscosity, Pa·s^{-1}.

By generating additional terms at higher Reynolds numbers, the RNG k-ε model compensates for the shortcomings of the standard k-ε model. These are the reformed equations for k and ε:[55]

$$\frac{\partial}{\partial t}(\rho \mathrm{k}) + \nabla\cdot(\rho \mathrm{uk} - \mu_{eef}\sigma\nabla \mathrm{k}) = G_b + G_k - \rho\varepsilon - Y_m + S_k \quad (22)$$

$$\frac{\partial}{\partial t}(\rho\varepsilon) + \nabla\cdot(\rho \mathrm{u}\varepsilon - \mu_{eef}\sigma\nabla\varepsilon) = \frac{\varepsilon}{\mathrm{k}}(C_{\varepsilon 1}(G_k + G_b) - C_{\varepsilon 2}\rho\varepsilon) + S_\varepsilon - R_\varepsilon \quad (23)$$

R_ε: Correction term under different Re numbers.

In reactor simulations, the stirring shaft and paddle continuously move over time. Researchers have proposed a number of approaches to address the interaction between the revolving paddle and the stationary baffle. The internal and external iteration method, the "black box" model method, the sliding grid method (SM), the momentum source method, the multiple reference frames (MRF) method, and the rapid photography method are among these.[56−59]

Simulation has become an integral part of reactor research, and when combined with experimental studies, it can expedite the design and optimization of reactors significantly. Murthy et al.[34] utilized CFD to simulate the suction rate and power consumption of the self-inducing reactor, thereby significantly reducing the cost of experimentation. Simulation technology's ability to predict these computational parameters has significant implications for reactor and internal structure design. Achouri et al.[60] performed numerical simulations to examine the effect of impeller immersion depth and blade angle on the k_La of a self-inducing impeller in the reactor and compared the results to experimental data. Greater impeller depth and blade angle resulted in lower k_La values. Due to the diverse internal structures of reactors, it is essential to select the most applicable models for simulation and prediction purposes during simulation and optimization design. Li et al.[9] utilize the standard k-ε model to predict the gas self-induced flow rate, power consumption, and impeller power number of the hollow self-inducing impeller and contrast and discuss it with experimental data from the research that has been published. The outcomes demonstrate that the CFD results are highly reliable. Jahoda et al.[61] used the multiple reference frame (MRF) method and the sliding grid method (SM) to simulate single-phase and gas−liquid two-phase unsteady states, respectively, and they compared the parameters obtained from the two methods. The characteristics acquired using the two techniques in a single-phase system were mostly consistent. In a two-phase gas−liquid system, however, the SM demonstrated a greater correlation with experimental results. Due to the longer computational time required by the SM, Achour et al.[62] utilized a three-dimensional steady-state simulation method to simulate the pressure difference and flow field in the self-inducing reactor, thereby providing intuitive insights into the self-inducing reactor's suction principle.

Simulation serves a crucial role in accelerating the design of reactors. Utilizing experimental data, numerical simulation allows for the visualization of the phase distribution throughout the reaction process. In the context of self-inducing reactors, numerical modeling is of critical significance for making predictions about a wide range of parameters. By simulating these predictive parameters, the self-inducing performance can be evaluated effectively, and the suction process can be visualized. As a consequence, this provides a robust framework for the design and optimization of self-inducing structures.

3. APPLICATION OF SELF-INDUCING REACTORS

Due to their advantageous characteristics, such as high raw material utilization, efficiency, energy efficiency, and gas recovery capacities, self-inducing reactors have drawn significant attention among researchers. Consequently, extensive research has been conducted in various disciplines, resulting in substantial progress in this area of study.[63] In response to the expanding global demand for bioproducts, cell culture technology has grown in prominence, with bioreactors playing a crucial role. A favorable cell culture environment is indispensable for attaining high culture density and establishing the groundwork for large-scale bioproduct production. It is vital to reduce shear pressures as much as possible, provide effective mixing, and maximize ventilation in order to fulfill the prerequisites of cell culture. This will help to reduce the amount of cell damage that occurs while still guaranteeing enough nutrition. Kshirsagar et al.[64] developed a novel self-inducing agitated photobioreactor utilizing *Spirulina platensis* as a model system. As depicted in Figure 4, the reactor is

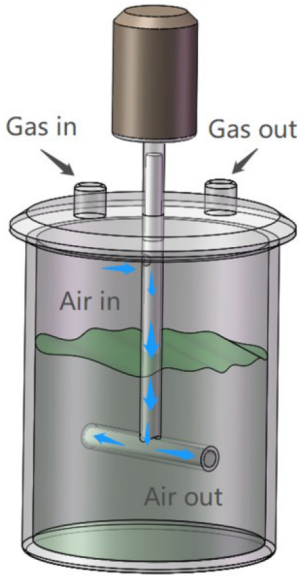

Figure 4. Novel self-inducing impeller milli upgrade bioreactor. The photobioreactor consists of a hollow tube self-inducing impeller. A hollow shaft above the liquid level has an air inlet hole, which is rotated to suck the gas in and disperse it in the reactor.

equipped with a self-inducing hollow-tube impeller. This design minimizes shear forces, facilitates byproduct recovery, and significantly improves biomass concentration and specific growth rate.

Puskeiler et al.[65] devised a unique self-inducing impeller milli-upgrade bioreactor with a high volumetric mass transfer coefficient. Batch culture experiments were performed by utilizing *Escherichia coli*, yielding noteworthy outcomes. The

https://doi.org/10.1021/acsomega.3c06484
ACS Omega 2023, 8, 48613−48624

growth rate and biological production of *Escherichia coli* in the 10 mL-size reactor exhibited similarity to those seen in a conventional agitator of a significantly higher scale, such as 3.0 L. The issue of global energy scarcity has emerged as a progressively urgent concern, prompting a heightened emphasis on the advancement of efficient, green, and renewable alternative fuels. Ethanol, being a cleaner fuel alternative, has superior performance compared to gasoline across multiple aspects. Nevertheless, conventional chemical catalytic techniques utilized in the synthesis of ethanol require the use of elevated temperature and pressure conditions. Moreover, these processes exhibit low selectivity and sensitivity toward the composition of synthetic gas components.[66] In response to these challenges, synthetic gas biological fermentation has emerged as a promising alternative for ethanol production. Specific strains of *Clostridium* bacteria possess the ability to transform carbon monoxide (CO) and hydrogen (H_2) into ethanol and acetic acid.[67] At present, stirred tank reactors (STRs) are widely utilized as the predominant bioreactors for the process of synthesis gas fermentation. Nevertheless, the insufficient mass transfer efficiency of stirred tank reactors (STRs) is frequently seen as a result of the limited solubility of CO and H_2 in liquid media. In order to enhance mass transfer, STRs commonly employ strategies such as augmenting impeller speed and ventilation rate.[68,69] However, this methodology may lead to elevated energy consumption and the production of shear pressures that might have adverse effects on microorganisms. Hence, the use of self-inducing reactors presents a promising resolution by promoting the dissolution of CO and H_2, thereby augmenting the efficiency of mass transfer.

Self-inducing reactors have been shown to provide some benefits over typical stirring aeration reactors in specific aerobic biological fermentation operations. These reactors efficiently enable the necessary gas−liquid mixing and gas supply mechanisms for fermentation operations. They improve the effectiveness of dissolved oxygen and facilitate the internal circulation of unutilized gas. In research done by Wu et al.,[70] the simultaneous synthesis of ethanol and succinic acid was investigated utilizing two types of bioreactors: stirred aeration bioreactors and self-inducing bioreactors. The structural schematic is shown in Figure 5. The self-inducing impeller is employed to effectively redirect the CO_2 produced during ethanol synthesis for utilization in succinic acid production. The process of integration described herein serves to mitigate the environmental impact of ethanol production by reducing CO_2 emissions while simultaneously improving the efficiency of CO_2 usage in the manufacture of succinic acid.

Gas−liquid reactions are prevalent chemical processes in the realm of industrial manufacturing. Nevertheless, conventional stirred tank reactors commonly employ bubbling via a ventilation pipeline, leading to inadequate dispersion of bubbles. This constraint has an adverse effect on both the rates of reactions and the resulting yields. Moreover, unreacted gas is typically discharged as waste gas, resulting in a decrease in gas utilization efficiency. In order to address these challenges, researchers have investigated the employment of multicascade reactors as a means to facilitate efficient and rapid manufacturing. Self-inducing reactors have several benefits within the manufacturing process of diverse items. They can effectively conserve energy, enhance raw material utilization, and substantially reduce exhaust gas emissions in gas−liquid reactions. The attainment of equilibrium between shear stress and gas−liquid mixing has significant importance in the further progress of utilizing self-inducing reactors within the realm of bioengineering.

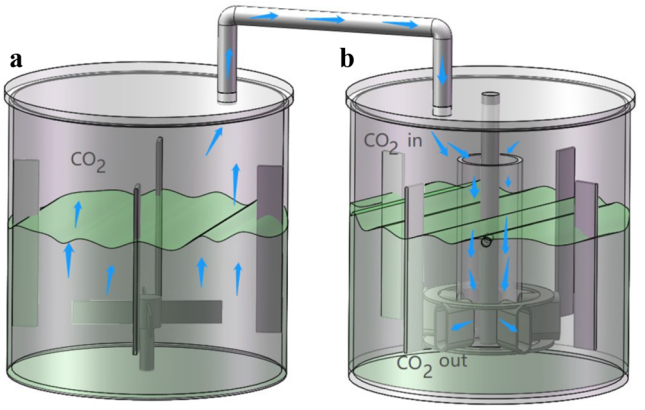

Figure 5. Schematic of ethanol-coupled succinic acid production. (a) Production of ethanol. (b) Generation of succinic acid. The system consists of a stirred bioreactor (a) and a self-inducing bioreactor (b). The CO_2 generated in the stirred bioreactor enters the self-inducing bioreactor through a pipeline and is absorbed and dispersed into the bioreactor under the action of an impeller for succinic acid production.

4. CONCLUSION AND PERSPECTIVES

The self-inducing reactor, characterized by its distinctive configuration, is extensively utilized in the realm of bioengineering and several other disciplines. In the study of self-inducing reactors, it is crucial to augment their configuration as well as enhance impeller design through theoretical investigation. The objective of this approach is to enhance the suction performance and mass transfer characteristics of the reactor. Impeller rotational speed is a limiting factor in the suction performance of a self-inducing reactor. Excessive rotational speed has the potential to induce heightened shear stresses, which can be detrimental to shear-stress-sensitive cultures, particularly those including microorganisms. Moreover, the dispersion efficiency of self-inducing reactors may be less than desirable. In order to address the aforementioned issues encountered in real industrial applications, it is common practice to integrate self-inducing impellers with other varieties of stirring impellers. This combination facilitates the achievement of multilayer stirring and self-induction. Furthermore, the integration of aeration with self-induction is employed in bioengineering reactors to augment the overall efficiency of mixing and mass transfer processes. This approach ensures the efficacy of the self-inducing impeller in terms of suction performance and mixing characteristics. Additionally, it leads to a reduction in exhaust emissions, an enhancement in gas circulation efficiency, a decrease in expenses, and a mitigation of environmental contamination. The accurate prediction of the internal flow field within the reactor is of utmost importance, as it undergoes alterations in response to changes in the reactor's construction. Continuous fermentation has attracted increasing interest in recent times. In contrast to batch fermentation, continuous fermentation has the potential to enhance equipment utilization rate and output per unit time while also reducing nonproduction time in the reaction process. Hence, the utilization of multistage reactors holds significant potential across a wide range of applications. The use of gas inside self-inducing reactors is highly efficient,

https://doi.org/10.1021/acsomega.3c06484
ACS Omega 2023, 8, 48613−48624

and the integration of self-inducing reactors with other reactor types has considerable importance in enabling multistage utilization. The visualization of the internal flow field of the reactor may be achieved through the utilization of CFD technology. The integration of experimental research and computer simulation facilitates the rectification of scale-up parameters within the design phase. This integrated approach provides reliable information for optimizing and designing reactors in bioengineering.

AUTHOR INFORMATION

Corresponding Author

Hui Li − *College of Biotechnology and Pharmaceutical Engineering, State Key Laboratory of Materials-Oriented Chemical Engineering, Nanjing Tech University, Nanjing 211816, China;* orcid.org/0000-0002-5139-2919; Email: lihui11@njtech.edu.cn

Authors

Jian Gan − *College of Biotechnology and Pharmaceutical Engineering, State Key Laboratory of Materials-Oriented Chemical Engineering, Nanjing Tech University, Nanjing 211816, China*

Huazong Liu − *College of Biotechnology and Pharmaceutical Engineering, State Key Laboratory of Materials-Oriented Chemical Engineering, Nanjing Tech University, Nanjing 211816, China*

Jiajun Chen − *College of Biotechnology and Pharmaceutical Engineering, State Key Laboratory of Materials-Oriented Chemical Engineering, Nanjing Tech University, Nanjing 211816, China*

Xingyan Li − *College of Biotechnology and Pharmaceutical Engineering, State Key Laboratory of Materials-Oriented Chemical Engineering, Nanjing Tech University, Nanjing 211816, China*

Ganlu Li − *College of Biotechnology and Pharmaceutical Engineering, State Key Laboratory of Materials-Oriented Chemical Engineering, Nanjing Tech University, Nanjing 211816, China*

Kequan Chen − *College of Biotechnology and Pharmaceutical Engineering, State Key Laboratory of Materials-Oriented Chemical Engineering, Nanjing Tech University, Nanjing 211816, China;* orcid.org/0000-0001-8432-7032

Complete contact information is available at: https://pubs.acs.org/10.1021/acsomega.3c06484

Notes

The authors declare no competing financial interest.

ACKNOWLEDGMENTS

This work was supported by the National Key Research and Development Program of China (2018YFA0901500), National Natural Science Foundation of China (22378200), Basic Science (Natural Science) Research Project of Jiangsu Province Colleges and Universities (21KJB530014), and Jiangsu Synergetic Innovation Center for Advanced Bio-Manufacture.

ABBREVIATIONS

MRF	Moving reference frame
rpm	Revolutions per minute
SM	Sliding grid method

NOMENCLATURE

c	Dimensionless constant, dimensionless
C_0	Conventional orifice coefficient, dimensionless
C_P	Pressure coefficient, dimensionless
C_ε	Additional generating term of equation, dimensionless
d	Impeller diameter, m
D	Reactor diameter, m
Fr	Froude number, dimensionless
Fr^*	Modified Froude number, dimensionless
g	Gravity acceleration, m·s^{-2}
G_b	Turbulence kinetic energy produced by buoyancy, J·kg^{-1}
G_K	Turbulence kinetic energy produced by average velocity gradient, J·kg^{-1}
h	Fluid unit position, m
h_0	Liquid depth, m
K	Velocity loss coefficient, dimensionless
K_0	Blade slip factor, dimensionless
K_1	Experimental constant, dimensionless
N	Impeller speed, r·min^{-1}
n_1	Number of blades, dimensionless
N_C	Critical speed, r·min^{-1}
N_p	Power number, dimensionless
N_{Re}	Reynolds number, dimensionless
P	Pressure at a certain point in a fluid, Pa
p and q	Subscripts p and q mean gas phase and liquid phase
P_1	Pressure at gas outlet, Pa
P_a	Gas suction inlet pressure, Pa
P_p	Power consumption during suction, W
Q	Gas suction rate, m^3·h^{-1}
R	Position of air outlet from rotating shaft, m
r_d	Bubble radius at detachment, m
R_ε	Correction term under different Re numbers
S	Air outlet area, m^2
S_k	Source term of k equation, kg·(m^3·s)$^{-1}$
S_ε	Source term of ε equation, kg·(m^3·s)$^{-1}$
t	Time, s
t_d	Total bubble formation time, s
u	Gas−liquid relative velocity at air outlet $u = \pi dNK$ $(0 < K < 1)$, m·s^{-1}
v	Velocity, m·s^{-1}
V_q	Liquid volume, m^3
V_{tip}	Speed of impeller tip, m·s^{-1}
y	Distance between the impeller and the tank bottom, m
Y_m	Influence of wave expansion on turbulent dissipation rate
α	Phase hold-up, %
ΔP	Pressure drop, Pa
ε	Turbulence dissipation rate, m^2·s^{-3}
μ	Viscosity, Pa·s^{-1}
μ_{eef}	Effective viscosity, Pa·s^{-1}
ρ	Density, kg·m^{-3}
σ	Turbulent Prandtl number, dimensionless
$\vec{F}_{lift,q}$	Lift force, N
$\vec{F}_q$	External forces, N
$\vec{F}_{td,q}$	Turbulent dispersion force, N
$\vec{F}_{wl,q}$	Wall slip force, N
$\vec{R}_{pq}$	Interphase drag, N
$\dot{m}_{pq}$ and $\dot{m}_{qp}$	Mass flow rate between two phases, kg·s^{-1}

https://doi.org/10.1021/acsomega.3c06484
ACS Omega 2023, 8, 48613−48624

$\overline{\tau}_q$	Stress tensor of q-phase, dimensionless
h_{f1}	Energy loss in turbulent liquid, dimensionless
h_{f2}	Energy loss in the flow process, dimensionless
S_1	Quality source term, $kg\cdot(m^3\cdot s)^{-1}$
λ_q	Bulk viscosity, $Pa\cdot s^{-1}$
μ_q	Shear viscosity, $Pa\cdot s^{-1}$

REFERENCES

(1) Torcida, M. F.; Curto, D.; Martin, M. Design and optimization of CO_2 hydrogenation multibed reactors. *Chem. Eng. Res. Des.* **2022**, *181*, 89−100.

(2) Ye, Q.; Li, Z.; Wu, H. Principle and performance of gas self-inducing reactors and applications to biotechnology. *Adv. Biochem. Eng. Biot.* **2015**, *152*, 1−33.

(3) Gao, Z.; Bai, Y.; Su, J. Manganese redox cycling in immobilized bioreactors for simultaneous removal of nitrate and 17β-estradiol: Performance, mechanisms and community assembly potential. *Bioresour. Technol.* **2023**, *367*, No. 128282.

(4) Zheng, Z.; Ali, A.; Su, J.; Zhang, S.; Su, L.; Qi, Z. Biochar fungal pellet based biological immobilization reactor efficiently removed nitrate and cadmium. *Chemosphere.* **2022**, *296*, No. 134011.

(5) Aalto, S. L.; Suurnakki, S.; von Ahnen, M.; Tiirola, M.; Pedersen, P. B. Microbial communities in full-scale woodchip bioreactors treating aquaculture effluents. *J. Environ. Manage.* **2022**, *301*, No. 113852.

(6) Scargiali, F.; Tamburini, A.; Caputo, G.; Micale, G. On the assessment of power consumption and critical impeller speed in vortexing unbaffled stirred tanks. *Chem. Eng. Res. Des.* **2017**, *123*, 99−110.

(7) Saravanan, K.; Patwardhan, A. W.; Joshi, J. B. Critical impeller speed for solid suspension in gas inducing type mechanically agitated contactors. *Can. J. Chem. Eng.* **1997**, *75*, 664−676.

(8) Mundale, V. D.; Joshi, J. B. Optimization of impeller design for gas inducing type mechanically agitated contactors. *Can. J. Chem. Eng.* **1995**, *73*, 161−172.

(9) Li, L.; Chen, N.; Xiang, K. CFD simulation of hydrodynamics characteristics in a tank stirred by a hollow self-inducing impeller. *Can. J. Chem. Eng.* **2018**, *96* (8), 1837−1848.

(10) Kasundra, R. B.; Kulkarni, A. V.; Joshi, J. B. Hydrodynamic and mass transfer characteristics of single and multiple impeller hollow self-inducing reactors. *Ind. Eng. Chem. Res.* **2008**, *47* (8), 2829−2841.

(11) Poncin, S.; Nguyen, C.; Midoux, N. Hydrodynamics and volumetric gas−liquid mass transfer coefficient of a stirred vessel equipped with a gas-inducing impeller. *Chem. Eng. Sci.* **2002**, *57* (16), 3299−3306.

(12) Yang, C.; Luo, G.; Yuan, X.; Chen, J.; Lu, Y.; Tang, X. Numerical simulation and experimental investigation of multiphase mass transfer process for industrial applications in China. *Rev. Chem. Eng.* **2019**, *36*, 187−214.

(13) Saravanan, K.; Mundale, V. D.; Joshi, J. B. Gas inducing type mechanically agitated contactors. *Ind. Eng. Chem. Res.* **1994**, *33*, 2226−2241.

(14) Saravanan, K.; Joshi, J. B. Gas-inducing-type mechanically agitated contactors: hydrodynamic characteristics of multiple impellers. *Ind. Eng. Chem. Res.* **1995**, *34*, 2499−2514.

(15) Sardeing, R. F.; Poux, M.; Xuereb, C. Development of a new gas-inducing turbine family: The partially shrouded turbine. *Ind. Eng. Chem. Res.* **2006**, *45* (13), 4791−4804.

(16) Dhaouadi, H.; Poncin, S.; Midoux, N.; Wild, G. Gas−liquid mass transfer in an airlift reactor—analytical solution and experimental confirmation. *Chem. Eng. Process.* **2001**, *40* (2), 129−133.

(17) Gomadurai, C.; Saravanan, K.; Abraham, E.; Deepa, N. Hydrodynamic studies on air-inducing impeller system. *Int. J. Chemtech. Res.* **2014**, *6*, 4471−4474.

(18) Achouri, R.; Hamza, S. B.; Dhaouadi, H.; Mhiri, H.; Bournot, P. Volumetric mass transfer coefficient and hydrodynamic study of a new self-inducing turbine. *Energy. Convers. Manag.* **2013**, *71*, 69−75.

(19) Forrester, S. E.; Rielly, C. D. Modelling the increased gas capacity of self-inducing impellers. *Chem. Eng. Sci.* **1994**, *49*, 5709−5718.

(20) Heim, A.; Krasawski, A.; Rzyski, E.; Stelmach, J. Aeration of bioreactors by self-aspirating impellers. *Chem. Eng. J.* **1995**, *58* (1), 59−63.

(21) Forrester, S. E.; Rielly, C. D.; Carpenter, K. J. Gas-inducing impeller design and performance characteristics. *Chem. Eng. Sci.* **1998**, *53*, 603−615.

(22) Murthy, B. N.; Kasundra, R. B.; Joshi, J. B. Hollow self-inducing impellers for gas−liquid−solid dispersion: Experimental and computational study. *Chem. Eng. J.* **2008**, *141* (1−3), 332−345.

(23) Ju, F.; Cheng, Z.; Chen, J.; Chu, X.; Zhou, Z.; Yuan, P. A novel design for a gas-inducing impeller at the lowest critical speed. *Chem. Eng. Res. Des.* **2009**, *87* (8), 1069−1074.

(24) Tanaka, M.; Noda, S.; Oshima, E. Effect of location of submerged impeller on entrainment of air bubbles from the free surface in a stirred vessel. *Kagaku Kogaku Ronbunshu* **1984**, *10*, 527−530.

(25) Bujalski, W.; Jaworski, Z.; Nienow, A. W. CFD study of homogenization with dual Rushton turbines—Comparison with experimental results: Part II: The multiple reference frame. *Chem. Eng. Res. Des.* **2002**, *80*, 97−104.

(26) Harvey, A. D., III; Rogers, S. E. Steady and unsteady computation of impeller-stirred reactors. *AIChE J.* **1996**, *42* (10), 2701−2712.

(27) Zhang, Y.; Zhang, Z.; Wei, C.; Wang, H. Critical impeller speeds for a gas-inducing stirring tank loaded with solid particles. *Chin. J. Chem. Eng.* **2018**, *26*, 1423−1429.

(28) Evans, G. M.; Rielly, C. D.; Davidson, J. F.; Carpenter, K. J. Hydrodynamic characteristics of a gas-inducing impeller. *Fluid. Mech. Mix. Mode. Oper. Exp. Technol.* **1992**, *10*, 153−161.

(29) Martin, G. Q. Gas-inducing agitator. *Ind. Eng. Chem. Process. Des. Dev.* **1972**, *11* (3), 397−404.

(30) Sawant, S. B.; Joshi, J. B. Critical impeller speed for the onset of gas induction in gas-inducing types of agitated contactors. *Chem. Eng. J.* **1979**, *18* (1), 87−91.

(31) Patil, S. S.; Mundale, V. D.; Joshi, J. B. Mechanism of gas induction in a self-inducting impeller. *Ind. Eng. Chem. Res.* **2005**, *44* (5), 1322−1328.

(32) Deshmukh, N. A.; Patil, S. S.; Joshi, J. B. Gas induction characteristics of hollow self-inducing impeller. *Chem. Eng. Res. Des.* **2006**, *84* (2), 124−132.

(33) Fonte, C. P.; Pinho, B. S.; Santos-Moreau, V.; Lopes, J. C. B. Prediction of the Induced Gas Flow Rate from a Self-Inducing Impeller with CFD. *Chem. Eng. Technol.* **2014**, *37* (4), 571−579.

(34) Murthy, B. N.; Deshmukh, N. A.; Patwardhan, A. W.; Joshi, J. B. Hollow self-inducing impellers: Flow visualization and CFD simulation. *Chem. Eng. Sci.* **2007**, *62*, 3839−3848.

(35) Stitt, E. H. Alternative multiphase reactors for fine chemicals: a world beyond stirred tanks. *Chem. Eng. J.* **2002**, *90* (1−2), 47−60.

(36) Zieverink, M. M. P.; Kreutzer, M. T.; Kapteijn, F.; Moulijn, J. A. Gas− Liquid Mass Transfer in Benchscale Stirred Tanks Fluid Properties and Critical Impeller Speed for Gas Induction. *Ind. Eng. Chem. Res.* **2006**, *45*, 4574−4581.

(37) Linek, V.; Vacek, V.; Beneš, P. A critical review and experimental verification of the correct use of the dynamic method for the determination of oxygen transfer in aerated agitated vessels to water electrolyte solutions and viscous liquids. *Chem. Eng. J.* **1987**, *34* (1), 11−34.

(38) Nocentini, M. Mass transfer in gas-liquid, multiple-impeller stirred vessels: a discussion about experimental techniques for KLa measurement and models comparison. *Chem. Eng. Res. Des.* **1990**, *68* (3), 287−294.

(39) Sharma, H.; Nirmalkar, N. Enhanced gas-liquid mass transfer coefficient by bulk nanobubbles in water. *Mater. Today.* **2022**, *57*, 1838−1841.

https://doi.org/10.1021/acsomega.3c06484
ACS Omega 2023, 8, 48613−48624

(40) Lakhdissi, E. M.; Fallahi, A.; Guy, C.; Chaouki, J. Effect of solid particles on the volumetric gas liquid mass transfer coefficient in slurry bubble column reactors. *Chem. Eng. Sci.* **2020**, *227*, No. 115912.
(41) Yu, H.; Tan, Z. New correlations of volumetric liquid-phase mass transfer coefficients in gas-inducing agitated tank reactors. *Int. J. Chem. React. Eng.* **2012**, *10* (1), DOI: 10.1515/1542-6580.3049.
(42) Saravanan, K.; Joshi, J. B. Fractional gas hold-up in gas inducing type of mechanically agitated contactors. *Can. J. Chem. Eng.* **1996**, *74*, 16−30.
(43) Patil, S. S.; Joshi, J. B. Optimum design of multiple-impeller self-inducing system. *Ind. Eng. Chem. Res.* **2003**, *42* (6), 1261−1265.
(44) Doucet, L.; Ascanio, G.; Tanguy, P. A. Hydrodynamics characterization of rotor-stator mixer with viscous fluids. *Chem. Eng. Res. Des.* **2005**, *83* (10), 1186−1195.
(45) Baczkiewicz, J.; Michalski, M. Oxygen transfer during mixing of acetic acid fermentation medium with selfaspirating tube agitator. *Proceedings 6th European Conference on Mixing, Pavia.* **1988**, *6*, 473−478.
(46) Jafari, M.; Mohammadzadeh, J. S. S. Power consumption and onset speed for gas induction in a gas-induced contactor. *Chem. Eng. J.* **2004**, *103* (1−3), 1−5.
(47) Wang, Z.; Xu, P.; Li, X.; Wang, S.; Cheng, Z.; Ju, F. Impact of liquid driving flow on the performance of a gas-inducing impeller. *Chem. Eng. Process.* **2013**, *69*, 63−69.
(48) Zhang, T. W.; Wang, J. F.; Luo, Z.; Jin, Y. Spatial profiles of gas holdup in a novel internal-loop airlift reactor. *New Development and Application in Chemical Reaction Engineering.* **2006**, *159*, 521−524.
(49) Lo, C. S.; Hwang, S. J. Local hydrodynamic properties of gas phase in an internal-loop airlift reactor. *Chem. Eng. J.* **2003**, *91* (1), 3−22.
(50) Hampel, U.; Hristov, H. V.; Bieberle, A.; Zippe, C. Application of high-resolution gamma ray tomography to the measurement of gas hold-up distributions in a stirred chemical reactor. *Flow. Meas. Instrum.* **2007**, *18*, 184−190.
(51) Matsumura, M.; Sakuma, H.; Yamagata, T.; Kobyashi, J. Gas entrainment in a new gas entraining fermentor. *J. Ferment Technol.* **1982**, *60* (5), 457−467.
(52) Matsumura, M.; Umemoto, K.; Shinabe, K.; Kobyashi, J. Application of pure oxygen in a new gas entraining fermentor. *J. Ferment. Technol.* **1982**, *60* (6), 565−578.
(53) Petitti, M.; Vanni, M.; Marchisio, D. L.; Buffo, A.; Podenzani, F. Simulation of coalescence, break-up and mass transfer in a gas−liquid stirred tank with CQMOM. *Chem. Eng. J.* **2013**, *228*, 1182−1194.
(54) Launder, B. E.; Spalding, D. B. Mathematical Models of Turbulence. *Academic Press. J. Fluid. Mech.* **1972**, *57* (4), 826−828.
(55) Yakhot, V.; Orszag, S. A. Renormalization group analysis of turbulence. I. Basic theory. *J. Sci. Comput.* **1986**, *1*, 3−51.
(56) Pericleous, K. A.; Patel, M. K. The source-sink approach in the modeling of stirred reactors. *Physicochem. Hydrodyn.* **1987**, *9* (1−2), 279−297.
(57) Middleton, J. C.; Pierce, F.; Lynch, P. M. Computations of flow fields and complex reaction yield in turbulent stirred reactors, and comparison with experimental data. *Chem. Eng. Res. Des.* **1986**, *64*, 18−22.
(58) Micale, G.; Brucato, A.; Grisafi, F.; Ciofalo, M. Prediction of flow fields in a dual-impeller stirred vessel. *AIChE. J.* **1999**, *45*, 445−464.
(59) Gimbun, J.; Rielly, C. D.; Nagy, Z. K. Modelling of mass transfer in gas−liquid stirred tanks agitated by Rushton turbine and CD-6 impeller: A scale-up study. *Chem. Eng. Res. Des.* **2009**, *87*, 437−451.
(60) Achouri, R.; Dhaouadi, H.; Mhiri, H.; Bournot, P. Numerical and experimental investigation of the self-inducing turbine aeration capacity. *Energy. Convers. Manage.* **2014**, *83*, 188−196.
(61) Jahoda, M.; Tomášková, L.; Moštěk, M. CFD prediction of liquid homogenisation in a gas−liquid stirred tank. *Chem. Eng. Res. Des.* **2009**, *87* (4), 460−467.
(62) Achouri, R.; Mokni, I.; Mhiri, H.; Bournot, P. A 3D CFD simulation of a self inducing Pitched Blade Turbine Downflow. *Energy. Convers. Manage.* **2012**, *64*, 633−641.
(63) Hristov, H. V.; Stephan, B.; Uwe, H.; Holger, K.; Gunther, H.; Wilfried, S. A study on the two-phase flow in a stirred tank reactor agitated by a gas-inducing turbine. *Chem. Eng. Res. Des.* **2008**, *86* (1), 75−81.
(64) Kshirsagar, H. H.; Revankar, M. S.; Kamat, M. Y.; Lele, S. S. Cultivation of *Spirulina* in Gas Induced Photobioreactor and Isolation of Phycobiliproteins. *Indian. J. Biotechnol.* **2002**, *1* (3), 255−262.
(65) Puskeiler, R.; Kaufmann, K.; Weuster-Botz, D. Development, parallelization, and automation of a gas-inducing milliliter-scale bioreactor for high-throughput bioprocess design (HTBD). *Biotechnol. Bioeng.* **2005**, *89* (5), 512−523.
(66) Phillips, J. R.; Clausen, E. C.; Gaddy, J. L. Synthesis gas as substrate for the biological production of fuels and chemicals. *Appl. Biochem. Biotechnol.* **1994**, *45*, 145−157.
(67) Klasson, K. T.; Elmore, B. B.; Vega, J. L.; Ackerson, M. D.; Clausen, E. C.; Gaddy, J. L. Biological production of liquid and gaseous fuels from synthesis gas. *Appl. Biochem. Biotechnol.* **1990**, *24*, 857−873.
(68) Bredwell, M. D.; Worden, R. M. Mass-transfer properties of microbubbles. 1. Experimental studies. *Bio. Progress.* **1998**, *14* (1), 31−38.
(69) Bredwell, M. D.; Srivastava, P.; Worden, R. M. Reactor design issues for synthesis-gas fermentations. *Bio. Progress.* **1999**, *15* (5), 834−844.
(70) Wu, H.; Li, Q.; Li, Z.; Ye, Q. Succinic acid production and CO_2 fixation using a metabolically engineered Escherichia coli in a bioreactor equipped with a self-inducing agitator. *Bioresour. Technol.* **2012**, *107*, 376−384.

https://doi.org/10.1021/acsomega.3c06484
ACS Omega 2023, 8, 48613−48624